Clinical Oral Investigations (2022) 26:1053–1065
https://doi.org/10.1007/s00784-021-04089-y

ORIGINAL ARTICLE

Texturized P(VDF-TrFE)/BT membrane enhances bone neoformation in calvaria defects regardless of the association with photobiomodulation therapy in ovariectomized rats

Fernanda Cristina Toloi Rufato[1] · Luiz Gustavo de Sousa[1] · Priscilla Hakime Scalize[1] · Rossano Gimenes[2] · Isabela Hallak Regalo[1] · Adalberto Luiz Rosa[3] · Marcio Mateus Beloti[1] · Fabíola Singaretti de Oliveira[3] · Karina Fittipaldi Bombonato-Prado[1] · Simone Cecilio Hallak Regalo[1] · Selma Siéssere[1]

Received: 1 May 2021 / Accepted: 17 July 2021 / Published online: 9 August 2021

Abstract

Objectives The purpose of this investigation was to evaluate in vivo the response of bone tissue to photobiomodulation when associated with texturized P(VDF-TrFE)/BT in calvaria defects of ovariectomized rats.

Materials and methods Wistar Hannover rats were submitted to ovariectomy/control surgery. Calvaria bone defects of 5-mm diameter were performed after 90 days of ovariectomy. The animals were divided into OVX (without laser (L) and membrane), OVX + P(VDF-TrFE)/BT, OVX + P(VDF-TrFE)/BT + L, and OVX + PTFE + L. It was utilized a low-intensity gallium-aluminum-arsenide laser (GaAlAs) with 780-nm wavelength and 30-J/cm^2 energy density in 12 sessions (120 s). Thirty days after the bone defect the animals were euthanized for histological, microtomographic, and molecular evaluation. Quantitative analysis was analyzed by statistical software for $p < 0.05$.

Results Histological parameters showed bone tissue formation at the borders of all group defects. The association of photobiomodulation and texturized P(VDF-TrFE)/BT was not synergistic and did not show significant changes in morphometric analysis and biomarkers gene expression. Nevertheless, texturized P(VDF-TrFE)/BT membrane enhanced bone repair regardless of the association with photobiomodulation therapy, with an increase of connectivity density when compared to the OVX + PTFE + L group. The association of photobiomodulation therapy and PTFE was synergistic, increasing the expression of *Runx2*, *Alp*, *Bsp*, *Bglap*, *Sp7*, and *Rankl*, even though not enough to reflect significance in the morphometric parameters.

Conclusions The utilization of texturized P (VDF-TrFE)/BT, regardless of the association with photobiomodulation therapy, enhanced bone repair in an experimental model of osteoporosis.

Keywords Bone regeneration · Osteoporosis · Ovariectomy · Photobiomodulation · PBM · Vinylidene fluoride-trifluoroethylene copolymer

Introduction

Osteoporosis is a systemic and degenerative disease characterized by bone mass decrease and deterioration of trabecular microarchitecture leading to bone fragility and risk of fractures [1]. Its evolution is many times silent, nevertheless promoting an imbalance between osteoblastic and osteoclastic activity with subsequent implications [1, 2]. Osteoporosis affects the jaws [3], which can be a problem for dental practitioners because bone mass quality and quantity are both essential for the success of any restorative procedure.

Former reports have already demonstrated the association between osteoporosis and periodontal disease [3–6], corroborating the relationship between tooth decay and alveolar bone loss [3, 7–13]. Osteoporosis is a worldwide health issue and protocols that can favor bone tissue repair are necessary. Thus, in dentistry, two techniques have been utilized for bone repair: photobiomodulation and guided bone regeneration (GBR).

The utilization of photobiomodulation to repair bone must be performed preferentially with near-infrared laser therapy

Clinical relevance Texturized P(VDF-TrFE)/BT membrane is an option for guided bone regeneration in dentistry field to enhance bone repair.

✉ Selma Siéssere
selmas@forp.usp.br

Extended author information available on the last page of the article

due to its high penetration depth in this tissue [14]. The application of near-infrared light activates light-sensitive ion channels, increasing the levels of Ca^{2+} and leading to reactive oxygen species (ROS) and cyclic AMP (cAMP) interaction with the calcium ions. Therefore, these activities may increase cell migration as well as its proliferation and differentiation [15].

Photobiomodulation increases the expression of genes such as transforming growth factor beta (TGF-β), bone morphogenetic protein (BMP), fibroblast growth factor (FGF), and runt-related transcription factor 2 (RUNX2), which can stimulate osteoblastic proliferation and differentiation besides contributing to angiogenesis and enhancement of new bone tissue deposition in the injury site [16, 17]. Experimental osteoporosis investigation models have observed that photobiomodulation is beneficial for bone repair [18–20].

Guided bone regeneration is based on the utilization of resorbable or non-resorbable membranes to avoid the migration of epithelial and connective tissue cells during bone matrix consolidation, allowing osteoprogenitor cells to colonize the site since they have a slow migration rate [21]. The non-reabsorbable polytetrafluoroethylene membranes (PTFE) are very effective and considered the gold standard in bone tissue stimulation [22–26]. Nevertheless, reports have demonstrated that poly(vinylidene fluoride-trifluoroethylene)/barium titanate (P(VDF-TrFE)/BT) membrane associates the mechanical properties of polymers with the biocompatibility of the ceramics and can be a promising alternative for bone neoformation [27–30]. Even though (P(VDF-TrFE)/BT) may stimulate bone formation, some characteristics such as smoothness, hardness, and friability could be improved. Thus, for this investigation, a flexible and texturized (P(VDF-TrFE)/BT) membrane was assembled.

With the knowledge that techniques such as photobiomodulation therapy and GBR have already shown promising results when utilized in an isolated way, we hypothesized that photobiomodulation could act synergistically with P(VDF-TrFE)/BT membrane, enhancing bone repair. The purpose of this investigation was to evaluate bone neoformation by histological, tomographic, and molecular parameters in calvaria defects performed in rats submitted to bilateral ovariectomy, associating photobiomodulation and P(VDF-TrFE)/BT membrane.

Material and methods

Membranes

Texturized membranes of P(VDF-TrFE)/BT were manufactured by Professor Rossano Gimenes from the Institute of Physics and Chemistry of Federal University of Itajubá (UNIFEI, Brazil) and PTFE membranes commercially available (Bionnovation®, Bauru, SP, Brazil) were utilized as control. The membranes were cut into disks with 5-mm diameter and sterilized previously to their placement in bone defects.

Synthesis of P(VDF-TrFE)/$BaTiO_3$ composites texturized membranes

Commercial $BaTiO_3$ containing 99.9% of purity and particle size < 2 μm, purchased from Sigma Aldrich (St. Louis, MO, USA), was employed in the formulation of the composite. Commercial $BaTiO_3$ powder was calcined on a tubular furnace at 1380 °C for 4 h. The process was carried out in air flux to decompose the residual $BaCO_3$ contamination present in the commercial powder. Calcined $BaTiO_3$ was milled employing a planetary ball mill using isopropyl alcohol. The resulting $BaTiO_3$ powder was characterized by X-ray diffraction patterns (DRX) recorded in the 2θ ranging from 20 to 70° with step width 0.02° and step time 0.5 s, CuKα radiation, using panalytical scanning X-ray diffractometer (Almelo, Netherlands) model X'Pert Pro. Fourier-transform infrared spectroscopy (FTIR) was employed to identify the presence of solvent traces, or reminiscent carbonates. FTIR measurement was carried out in a Perkin Elmer Spectrum 100 FTIR spectrometer, in a range of 4000–400 cm^{-1}, a resolution of 4 cm^{-1}, and 32 scans.

The synthesis of the composite was performed using P(VDF-TrFE) powder (FC20, Piezotech Arkema, Pierre-Benite, France) dispersed in 20 g/100 mL of dimethylformamide 99.8% (DMF) (Sigma Aldrich, St. Louis, MO, USA) at room temperature (25 °C). The P(VDF-TrFE) powder was solubilized in DMF employing a magnetic stirrer at 60 °C, and after the copolymer dissolution, the calcined $BaTiO_3$ powder was added to the solution. This dispersion was homogenized using a sonicator (model VCX 750, Sonics and Materials, Newtown, CT, USA) operating at 562-W power for 6 min (3 cycles, duration of cycle 2 min). To avoid overheating and solvent losses, the dispersion was maintained in an ice/water bath. This procedure was performed to ensure that powder agglomerates would be better homogenized and dispersed into a copolymer matrix.

The deposition of P(VDF-TrFE)/$BaTiO_3$/DMF solution was executed employing the spray coating method, using a commercial 5-mm airbrush gun connected to a compressed air supply operating with pressure working at 20 kgf/cm^2. P(VDF-TrFE)/$BaTiO_3$/DMF deposition was performed at a standardized distance from 30 mm of a recipient content distilled water. The X/Y movement of the airbrush was performed by an experimental machine using step motors controlled by Arduino (model UNO) board.

After the deposition process, the membranes were manually removed from the water surface and dried in an oven at

100 °C for 12 h under vacuum. The thickness of the deposited film was controlled by the deposition time and measured using a digital micrometer, which corresponds to a range of 10–20 μm. The dispersion flow rate was regulated according to the homogeneous distribution of the solution and the non-formation of crinkles.

The conformation and structural phases of the PVDF-TrFE composites were performed by Fourier-transform infrared spectroscopy (FTIR), employed to identify the β-phases of the material and confirm the piezoelectricity of the composite. FTIR measurement was carried out in a Perkin Elmer Spectrum 100 FTIR spectrometer, in a range of 4000–400 cm^{-1}, a resolution at 4 cm^{-1}, and 32 scans. The X-ray pattern (XRD) was acquired using a Panalytical Scanning Diffractometer (Almelo, Netherlands) model (X'Pert Pro), using CuKα radiation, with step width 0.02° and step time 0.5 s. Sample wettability of both groups was evaluated through contact angle measurements and obtained data were employed to estimate the surface hydrophilicity of the texturized surface.

The wettability experiments were analyzed by a sessile Easy Drop Shape Analyzer (Krüss GmbH. Hamburg, Germany). The volume of the drop was 10 μL of MEM media (GIBCO), and the contact angle was acquired on different positions over the sample surfaces, with the mean value provided after five measurements at room temperature.

Animals

This investigation was approved by Animal Research Committee (Protocol 2018.1.417.58.0.). There were utilized 200 g Hannover Wistar rats ($n=40$) at 8 weeks old from Central Bioterium of Ribeirão Preto Campus of University of São Paulo (USP). The animals were maintained in the bioterium of FORP-USP with controlled room temperature (23 °C and 24 °C), exhaustion system, and daily illumination of 12 h. The animals passed through an adaptation of 7 days before surgery and during all the experiments were kept in polyethylene boxes (three per box). Anesthesia protocol was standardized in all surgical procedures, with intramuscular administration of 10 mg/kg xylazine and 75 mg/kg ketamine. Skin suture was performed with silk thread 4.0 (Ethicon, J&J, Brazil) and a unique intramuscular administration of 0.2 mL/100 g Flunixin meglumine (Schering-Plough, Brazil) associated with 0,1 mL/100 g Pentabiotic (Fort Dodge®, Brazil).

Osteoporosis experimental model

Bilateral ovariectomy (OVX) was performed with 35 animals through ovary exposition and resection [20, 29, 31, 32]. Confirmation of ovariectomy effects was performed by estrous cycle and macroscopic exam of uterine atrophy [33]. Animals from the control group were submitted to ovariectomy protocol, with exposition and reinsertion of ovaries in the abdominal cavity. All animals received posterior sutures and were maintained in the bioterium for 90 days with water and food ad libitum.

Calvarial bone defects and membrane insertion

Bone defects were performed 90 days after ovariectomy [34] and ovary exposition. Animals were anesthetized and sagittally incised (1 cm) in calvaria with a 15-surgical blade for left parietal bone exposition and creation of a defect with 5-mm diameter and 1-mm length employing an implant engine device (Dentscler, Brazil) adjusted to 3000 rpm and a drill with the same dimensions of the defect. Abundant irrigation with 0,9% saline was performed to avoid excessive temperature with the immediate insertion of P(VDF-TrFE)/BT and PTFE membranes inside the defect.

Photobiomodulation

A gallium-aluminum-arsenide (GaAlAs) Twin Laser (Mm Optics; São Carlos, SP, Brazil) with the following specifications, i.e., maximal energy density of 315 J/cm^2, a voltage of 100 ~ 240 V, frequency of 50–60 Hz, a wavelength of 780 nm, and maximal optic potency of 70 mW, was utilized.

The animals were anesthetized following the formerly described protocol to perform each of the 12 sessions of photobiomodulation. Irradiation was performed 24 h after surgical protocol and repeated every 2 days. The application was performed in the area corresponding to bone defect after gentle palpation and skin traction. A potentiometer was utilized previously for laser application, to adjust the potency and radiation dose of the equipment.

The bone defect was irradiated in its borders, with contact in the perpendicular direction, employing the following conditions: energy density of 30 J/cm^2 [20], potency of 40 mW, in four sites for 30 s in the positions of 3, 6, 9, and 12 h. The total application time in each session was 120 s. The energy values deposited daily and accumulated in each site were respectively: 1.2 J, 4.8 J, and 57.6 J. The irradiance (energy intensity) was 0.2 W/cm^2. The utilized equipment presents a 5-mm-application spot with an area of 0.04 cm^2, producing continuous waves. As a safety measure, PVC plastic film was set in the active laser point was utilized to avoid diffusion of the light beam.

Euthanasia was performed 30 days after the creation of bone defect and calvaria samples were collected. Thus, the experimental groups were divided into control ($n=5$) and ovariectomized groups: ovariectomized (OVX, $n=5$), ovariectomized + P(VDF-TrFE)/BT ($n=10$), ovariectomized + P(VDF-TrFE)/BT + photobiomodulation (L) ($n=10$), and ovariectomized + PTFE + L ($n=10$). Samples

from the control and OVX groups were not submitted to quantitative gene expression analysis due to insufficient bone formation. Nevertheless, there were performed microtomographic and histological analyses. The other group samples were used to perform microtomographic and histological analysis besides quantitative gene expression analysis.

Microtomographical analysis (micro-CT)

Calvaria samples were fixed in buffered formaldehyde 4% (pH = 7) for 48 h followed by 70% ethanol for 3 days. For image acquisition, a micro-CT SkyScan 1172 (SkyScan, Belgium) equipment was utilized, which allows the acquisition of 2D images and 3D reconstructions using the software NRecon, essential for the analysis of parameters associated with the bone defect, recommended by the American Society of Bone and Mineral Research (ASBMR) and described by Parfitt et al. [35], Bouxsein et al. [36], and Dempster et al. [37]. Among the parameters generated by the software, the following were selected: bone volume (mm^3), bone surface (mm^2), trabecular number (1/mm), trabecular thickness (mm), trabecular separation (mm), and connectivity density ($1/mm^3$).

Histological analysis

After microtomographic image acquisition, the samples were prepared to perform histological slides of mineralized material. Crescent alcohol dehydration was performed, followed by inclusion in acrylic resin (LR White Hard Grade, London Resin Company Ltd., UK). The obtained blocks were centrally sectioned by precision microtome (Exakt, Germany) and ground and polished (Exakt polishing method). The polished face was glued on an acrylic slide Exakt and sectioned to obtain 40-µm of width with a final width of 20 µm after wearing and polishing. The samples were stained with Stevenel's blue and Alizarin red S [38]. Two slides from each sample were observed in a light microscope (Leika, Germany). For histological analysis, it was observed the neoformed bone area to identify immature or trabecular bone, presence of osteoid tissue, osteoblasts, osteocytes, and blood vessels [29, 39]. The presence of strange body reactions, multinucleated giant cells, and fibrous tissue encapsulation was also evaluated.

Quantitative gene expression by real-time PCR

The following expressions of osteoblastic markers were analyzed: Runt-related transcription factor 2 (*Runx2*), alkaline phosphatase (*Alp*), bone sialoprotein (*Bsp*), osteocalcin (*Bglap*), osteopontin (*Opn*), osterix (*Sp7*); receptor activator of nuclear factor-kappa-beta ligand (*Rankl*) and osteoprotegerin (*Opg*); and markers associated to osteoclast differentiation such as receptor activator of nuclear factor-kappa-beta (*Rank*), cathepsin K, matrix metalloproteinase-9 (*Mmp9*), and calcitonin receptor (*Ctr*).

The neoformed bone adjacent to the membranes was precisely collected using the same trephine bur utilized to perform the defects and irrigated with iced phosphate saline (PBS—Life Technologies, Carlsbad, CA, USA) minimizing the heating and degradation of total RNA. Thus, the samples contained only the neoformed tissue, without circumjacent normal tissue.

Furthermore, the samples were frozen in liquid nitrogen and stored in a freezer − 80 °C. It was performed the maceration of the samples and calcined in a dry oven at 180 °C for 6 h for RNases degradation [38] and liquid nitrogen was employed during the maceration of calcined samples to obtain a fine powder. All the protocols were performed employing real-time polymerase reaction using a TaqMan probe system and StepOne™ System (Thermofisher) as described by Oliveira et al. [33]. The concentration and purity of RNA were analyzed through a spectrophotometer (NanoVue Plus Spectrophotometer, GE, Sweden) to obtain the concentration of RNA/µL (260 nm), contamination by proteins (280 nm), and phenol (230 nm). Expression levels of the target gene samples were normalized by glyceraldehyde-3-phosphate dehydrogenase (*Gapdh*) constitutive gene. There were used $2^{-\Delta\Delta CT}$ methods for normalization and relative quantification of gene expression [40]. Table 1 lists the oligonucleotide primers used in qRT-PCRs primers for the selected mRNAs.

Total RNA quality was evaluated by microfluidic electrophoresis (Bioanalyzer 2100, Agilent, USA) with RNA 6000 Nano Chips (Agilent Technologies, USA) using the protocol described by Scalize et al. [29]. Samples with RIN values above 7.5 were considered viable for PCR assay.

Statistical analysis

Results obtained in microtomographic parameters and for osteoblastic and osteoclastic biomarkers were analyzed using statistical software GraphPad Prism 6.0 ($p < 0.05$). There were utilized ANOVA and Tukey post-test, after verification of data normal distribution (Shapiro–Wilk).

Results

Confirmation of ovariectomy

Samples collected during five consecutive days from vaginal fluid and observed in a light microscope showed a predominance of leucocytes corresponding to the diestrus phase. Besides, macroscopic evaluation of uterine horns showed

Table 1 TaqMan primers used in real-time PCR

Gene symbol	Gene name	TaqMan assay
Gapdh	Glyceraldehyde-3-phosphate dehydrogenase	Rn99999916_s1
Runx2	Runt-related transcription factor 2	Rn01512298_m1
Alpl	Alkaline phosphatase	Rn01516028_m1
Ibsp	Bone sialoprotein	Rn00561414_m1
Bglap	Bone gamma-carboxyglutamate protein	Rn00566386_g1
Spp1	Secreted phosphoprotein 1 (osteopontin/Opn)	Rn01449972_m1
SP7	Sp7 transcription factor (osterix/osx)	Rn02769744_s1
Opg	Tumor necrosis factor receptor superfamily member 11B (osteoprotegerin/Opg)	Rn00563499_m1
Rank	Receptor activator of nuclear factor κ B (rank)	Rn04340164_m1
Rankl	Receptor activator of nuclear factor-kappa-beta ligand	Rn00589289_m1
Ctsk	Cathepsin K	Rn00580723_m1
Mmp9	Matrix metallopeptidase 9	Rn00579162_m1
Ctr	Calcitonin receptor	Rn00562334_m1

atrophy and a greater quantity of adipose tissue, confirming the osteoporosis condition of the animals.

Histological analysis

In Fig. 1, there can be observed histological images of control (a), OVX (b); OVX + P(VDF) (c), OVX + P(VDF) + L (d), and OVX + PTFE + L (e) groups. It can be observed bone neoformation in the peripheral borders of the calvaria defect of the control group, with the other regions fulfilled with connective tissue. Ovariectomized group (OVX) presented less bone neoformation at the defect limits when compared to the control group, added by a greater amount of thick connective tissue. Adjacent to neoformed bone tissue, bulky and more round osteoblasts were observed in the control group when compared to more flattened ones in the OVX group.

The groups with the presence of membranes, e.g., OVX + P(VDF), OVX + P(VDF) + L, and OVX + PTFE + L, also showed neoformed bone tissue in the peripheral region of the defect besides the absence of inflammatory infiltrate in the healing site. The group OVX + P (VDF) showed osteocytes inside lacunas and considerable connective tissue adjacent to trabecular bone.

The only group indicating contact between the membrane and bone tissue was OVX + PTFE + L. All the groups with the membranes presented bone marrow intermediating trabeculae and osteocytes in the extracellular matrix.

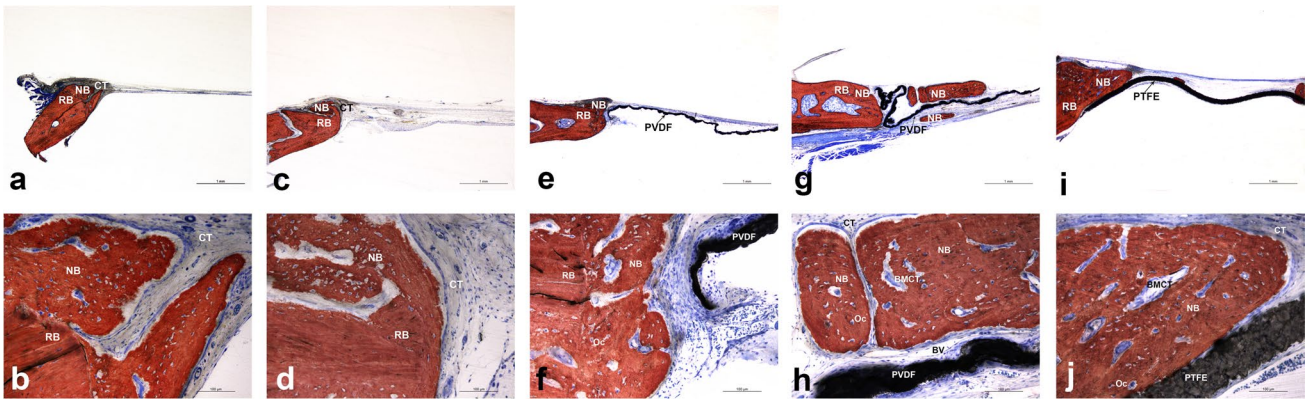

Fig. 1 Histological image of the control (a–b), OVX (c–d); OVX + P(VDF) (e–f), OVX + P(VDF) + L (g–h), and OVX + PTFE + L (i–j). RB, remaining bone; NB, neoformed bone; CT, connective tissue; Oc, osteocyte; PVDF, P(VDF-TrFE)/BT membrane; BMCT, bone marrow connective tissue; BV, blood vessel and PTFE, PTFE membrane. Barr magnication = 1 mm (a, c, e, g, i), and 100 µm (b, d, f, h, j)

Micro-CT analysis

Figure 2 illustrates the results of parameters associated with the bone defect obtained by micro-CT. When the groups that utilized the membranes (OVX + P (VDF), OVX + P(VDF) + L, and OVX + PTFE + L) were compared to the control group, bone volume was significantly higher for the groups that utilized membrane and/or membrane with photobiomodulation ($p < 0.05$). Similar behavior was observed for OVX + P(VDF), OVX + P(VDF) + L, and OVX + PTFE + L groups when compared to the OVX group ($p < 0.05$).

The bone surface had no statistical difference among the groups OVX + P(VDF), OVX + P(VDF) + L, and OVX + PTFE + L. Nevertheless, the same groups presented significantly higher values than the control and OVX groups ($p < 0.05$).

The trabecular number was similar among OVX + P(VDF), OVX + P(VDF) + L, and OVX + PTFE + L groups. These same groups presented significantly higher

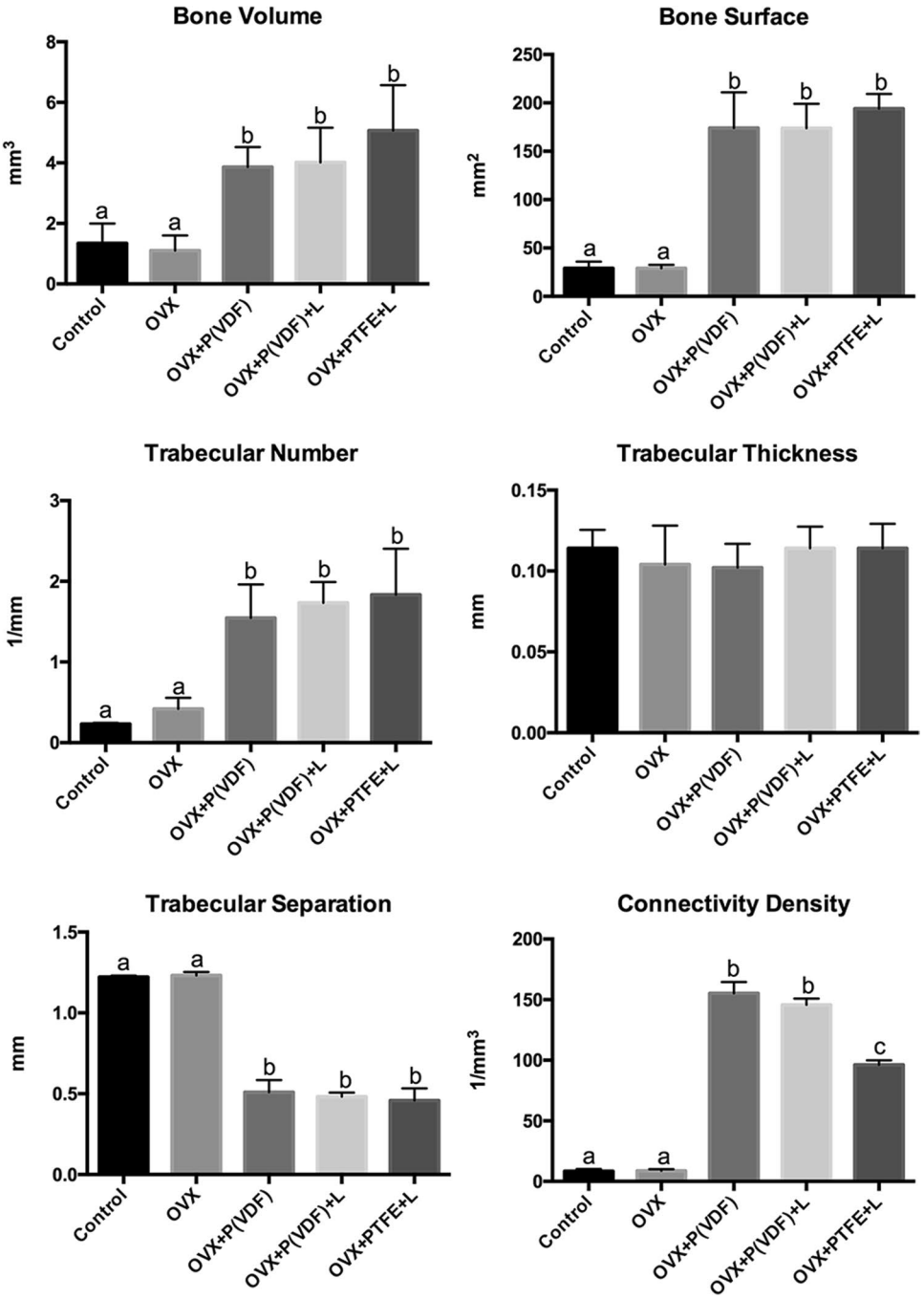

Fig. 2 Morphometric parameters obtained from microcomputed tomography images of bone defects of the evaluated groups. Different letters indicate statistical difference ($p < 0.05$)

values than the control ($p < 0.0001$ for comparison between groups) and OVX ($p < 0.05$) groups.

Trabecular thickness values were similar among the groups. Trabecular separation was significantly decreased for OVX + P(VDF), OVX + P(VDF) + L, and OVX + PTFE + L groups than in the control and OVX ($p < 0.05$) groups. In the same way, considering this parameter, there was no statistical difference among the OVX + P(VDF), OVX + P(VDF) + L, and OVX + PTFE + L groups.

The values for connectivity density were significantly higher in OVX + P(VDF) and OVX + P(VDF) + L groups compared to OVX + PTFE + L, control, and OVX ($p < 0.05$). Besides, groups OVX + PTFE + L group showed significantly higher connectivity density than groups control and OVX ($p < 0.05$) groups.

Quantitative gene expression of osteoblastic and osteoclastic bone markers

Gene expression for osteoblastic and osteoclastic markers was modulated by photobiomodulation and utilization of membranes in the defects. The results are illustrated in Fig. 3. Gene upregulation was observed in OVX + PTFE + L group when compared to OVX + P(VDF) and OVX + P(VDF) + L groups for *Runx2*, *Alp*, *Bglap*, *Sp7*, and *Rankl* ($p < 0.05$). The OVX + PTFE + L group also presented upregulation for *Bsp* when compared to OVX + P(VDF) and OVX + P(VDF) + L and the OVX + P(VDF) group presented upregulation when compared to OVX + P(VDF) + L ($p < 0.05$). The OVX + P(VDF) group presented upregulation of Spp1 compared to OVX + P(VDF) + L and OVX + PTFE + L groups as well as OVX + P(VDF) + L group when compared to OVX + PTFE + L ($p < 0.05$). The OVX + P(VDF) group presented upregulation of *Opg* when compared to OVX + P(VDF) + L and OVX + PTFE + L groups ($p < 0.05$).

Significant modulation of markers associated with osteoclast differentiation was also observed. When compared to OVX + P (VDF), OVX + P(VDF) + L, and OVX + PTFE + L groups, OVX + PTFE + L presented upregulation of Rank and calcitonin receptor (*Ctr*) ($p < 0.05$). Upregulation of cathepsin K (*Ctsk*) was observed in OVX + P(VDF) when compared to OVX + P(VDF) + L and OVX + PTFE + L groups ($p < 0.05$). Upregulation of MMP9 was also observed in the group OVX + P(VDF) when compared to OVX + P(VDF) + L and OVX + PTFE + L as well as in group OVX + PTFE + L when compared to OVX + P(VDF) + L ($p < 0.05$).

The ratio *Rankl/Opg* was significantly decreased in the group OVX + P(VDF) when compared to OVX + P(VDF) + L and OVX + PTFE + L groups ($p < 0.05$). The group OVX + PTFE + L presented the highest ratio among the studied groups, with a statistical difference when compared to OVX + P(VDF) + L group ($p < 0.05$) (Fig. 3).

Discussion

The results obtained in this study showed that bone neoformation occurred in the defects with the presence of the membranes with or without laser application, which can be confirmed by histological and morphometric results.

Literature has been demonstrating photobiomodulation benefits in bone repair [18, 19, 41] despite controversial discussion involving the variations in irradiation protocols. The protocol utilized in this study was based on former investigations, which demonstrated its effectivity on bone neoformation in ovariectomized rats [20] leading to an increase in osteocyte number [32].

In addition to photobiomodulation, guided regeneration technique presents positive results due to the utilization of occlusive membranes, which allow the creation of an adequate and protected site for the recruitment of osteoprogenitor cells with subsequent proliferation and osteoblast differentiation [42, 43].

Histological results obtained in the present study point out the fact that both membranes used in the investigation promoted bone tissue neoformation, associated or not to photobiomodulation, as seen with P(VDF) [28–30, 44]. In agreement to Lopes et al. [28], defects fulfilled with P(VDF-TrFE)/BT membrane presented neoformed bone tissue, with interposed connective tissue between bone and membrane. Despite that, these results are different from other reports [29]. The fact that there were performed some improvements in the composition of P(VDF-TrFE)/BT membrane such as increased flexibility and texturization might have resulted in the present histological results. P(VDF-TrFE)/BT membranes were very friable and constituted a problem at the moment of their insertion in the bone defect. Therefore, the option of utilizing a more flexible membrane facilitated its insertion without promoting its rupture. Besides, texturization led to a rougher surface to increase contact surface and adhesion of the proteins responsible for local cell fixation, favoring osseointegration. Even though P(VDF-TrFE)/BT membrane formerly evaluated in the study of Scalize et al. [29] presented a smooth surface, there was observed neoformed bone tissue above and beneath it, different from results observed in the present investigation in the groups P(VDF-TrFE)/BT and PTFE + L, which showed neoformed bone only under the membrane. On the other hand, texturized P(VDF-TrFE)/BT membrane associated with laser-induced bone trabeculae formation above and beneath itself. No inflammatory cells were seen in the groups that received the membranes, even though reports detected the presence of macrophages with high-density PTFE, suggesting that it is not completely bioinert [45]. The absence of inflammatory cells in the presence of PTFE in this investigation might be a

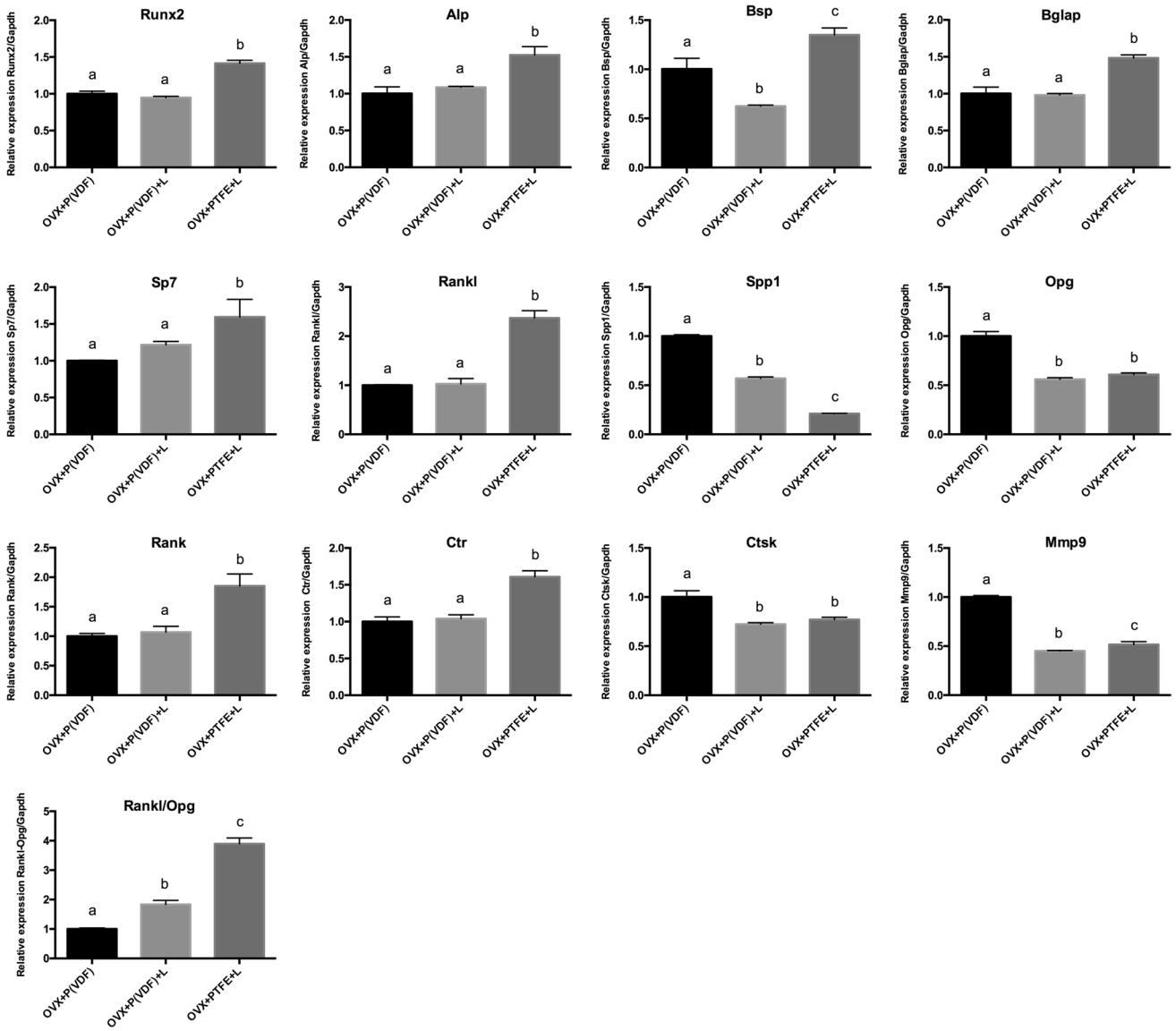

Fig. 3 Quantitative gene expression of osteoblastic markers, osteoclasts markers, and ratio *RANKL:OPG* of cells from new bone tissue formed on rat calvaria bone defect with membranes and/or membranes with laser. Gene expression was normalized by *Gapdh.* Different letters indicate statistical difference ($p < 0.05$)

consequence of its association with photobiomodulation, since it is known that this therapy might reduce inflammation [46].

The morphometric analysis by micro-CT proposed in the present study corroborates parameters preconized in the literature [36]. There was no statistical difference in bone volume, bone surface, trabecular number, trabecular separation, and trabecular thickness when comparing the groups that received the membranes with or without photobiomodulation therapy. Nevertheless, all these groups were different from the control and OVX regarding bone volume, bone surface, trabecular number, and trabecular separation, demonstrating that P(VDF-TrFE)/BT membrane was effective in inducing bone neoformation regardless of its association with photobiomodulation, as well as PTFE and photobiomodulation association.

Freitas et al. [47] observed increased bone neoformation with collagen membrane associated with photobiomodulation when compared to membrane alone, suggesting that photobiomodulation can be effective for bone repair when associated with guided regeneration techniques. These positive results might be due to different types of membranes or even to different irradiation protocols.

The bone neoformation that occurred in the defects with P(VDF-TrFE)/BT membrane might be explained by its piezoelectric property, i.e., the capacity of deformation with physiologic movements, and consequently, supply electric stimulation to cells and tissues without the need of an external source. Even in the absence of deformation, piezoelectric scaffolds exhibit protein adsorption and promote cell adhesion and proliferation, possibly because of permanent polarization and of charged surfaces of piezoelectric materials or transitory deformation caused by contraction and extrusion of adhered cells [48]. Bone is piezoelectric and the charges or potencies that generate in response to mechanical activity are capable of improving bone formation. Piezoelectric materials can stimulate the physiologic electrical environment and be a part of the stimulation of regeneration and repair [49], favoring osteoblastic differentiation [50].

The effectivity in bone neoformation is as important as the quality of the new bone associated with its resistance, which can be evaluated by measuring connectivity density. This parameter is important when analyzing osteoporosis development, mainly in women in the post-menopause period, where connectivity density diminishes, reducing bone resistance [51, 52]. When comparing the groups that received the membranes, there were observed higher values of connectivity density for the groups with P(VDF-TrFE)/BT associated or not with laser. These results are not in agreement with Scalize et al. [29] and we suggest that neoformed bone resulted from the presence of P(VDF-TrFE)/BT has better resistance when compared with laser associated with the PTFE membrane.

Biologic variation in gene expression might be an important molecular phenotype that can affect physiological parameters [53]. Cells obtained from bone tissue formed in the presence of membranes with or without laser were analyzed for osteoblastic biomarkers (*Runx2*, *Alp*, *Bsp*, *Bglap*, *Opn*, *Sp7*, *Opg*, and *Rankl*) as well as markers associated with osteoclast differentiation (*Rank*, *Ctsk*, *Mmp9*, and *Ctr*).

The group with PTFE membrane associated with photobiomodulation therapy presented induction in the expression of osteoblastic markers *Runx2*, *Alp*, *Bsp*, *Bglap*, *Osx*, and *Rankl* when compared to the groups P(VDF-TrFE)/BT and P(VDF-TrFE)/BT + L. In a former investigation conducted by our research group utilizing the same experimental model and the smooth-surfaced P(VDF-TrFE)/BT, we also observed a higher expression of *Runx2*, *Bsp*, *Osx*, and *Rankl* genes in the animals that received PTFE membrane [29].

The expression of *Runx2* was similar for the groups with P(VDF-TrFE)/BT associated or not with laser but was decreased when compared to group PTFE + L, suggesting that laser was not able to modulate its expression in the P(VDF-TrFE)/BT membrane. On the other hand, laser-induced *Runx2* expression with PTFE membrane in the present study, with superior results when compared to data from Scalize et al. [29], utilized the same membrane without laser association. The same expression pattern was observed for *Alp*, *Bglap*, *Sp7*, and *Rankl* in the evaluated groups. Oliveira et al. [54] have also observed an upregulation in the *Alp* gene in MCT3-E1 osteoblastic cells under therapy with GaAlAs laser of 780 nm as well as increased viability and cell differentiation. Alkaline phosphatase is among the first genes expressed in the process of extracellular mineralization [55] through the liberation of inorganic phosphate [56], and our results suggest that the association with photobiomodulation and PTFE membrane modulated positively this gene when compared to the other groups. Besides, the expression of *Alp*, *Bglap*, *Sp7*, and *Rankl* observed in the present investigation were superior when compared to PTFE without laser [29]. Another important gene associated with bone resorption that occurs with estrogen deficiency is *Rankl* [57] and its downregulation was best observed in the groups that received P(VDF-TrFE)/BT associated or not with laser. Bone sialoprotein (*Bsp*) is involved with the nucleation of hydroxyapatite crystals and osteoblast differentiation [58], and the present data show that association of P(VDF-TrFE)/BT with laser was prejudicial for the modulation of *Bsp* gene, being downregulated when compared to the presence of the membrane only. Besides, this gene was upregulated in the group PTFE associated with laser.

Osteopontin (*Spp1*) and osteocalcin (*Bglap*) act together as part of essential biological functions determining bone volume, shape, and resistance [59]. We have observed an upregulation of *Spp1* in the group with texturized P(VDF-TrFE)/BT and downregulation in the group with texturized P(VDF-TrFE)/BT associated with laser. This gene was also downregulated in the group with PTFE + L when compared to both former groups.

The main biological effect of osteoprotegerin (*Opg*) is to inhibit osteoclast differentiation and activation, favoring bone deposition. The utilization of P(VDF-TrFE)/BT led to an upregulation of *Opg* gene whereas the other groups that received laser therapy showed similar modulation. The upregulation of *Opg* in the presence of texturized P(VDF-TrFE)/BT membrane indicates osteoclastogenesis inhibition and therefore, protection against excessive tissue resorption [60]. Oliveira et al. [61] observed intense immunostaining of OPG with the association of AsGaAl diode laser to collagen sponge in bone defects of healthy rats, with an energy density of 120 J/cm^2 and potency of 50 mW. These researchers suggest that the utilization of collagen sponge associated with photobiomodulation could offer a synergic advantage to enhance bone repair, which was not observed in the present study.

The association of photobiomodulation with PTFE membrane upregulated the expression of *Rank*, calcitonin receptor, and *Mmp9*. Nevertheless, the highest values observed for cathepsin K (*Ctsk*) and *Mmp9* were in group

P(VDF-TrFE)/BT without photobiomodulation association. Even though these proteins have been associated with osteoclastic differentiation, investigations such as Mandelin et al. [62] observed that osteoblastic *Ctsk* may contribute to collagenous matrix maintenance and recycling of improperly processed collagen I. Besides, a recent study showed that periosteal stem cells (PSC) with *Ctsk* expression could contribute to mediate intramembranous bone formation [63, 64]. Former reports showed a molecular mechanism involved in osteoblast differentiation in vitro, requiring the expression of *Mmp9* [65], suggesting the important involvement of proteases in the extracellular matrix solubilization process, and its relationship with new bone formation [66]. This group also showed less *Rankl/Opg* ratio, suggesting a genetic modulation by the membrane and indicating that it can prevent bone resorption decreasing osteoclast activation in the repair site [29, 67].

Some limitations of the present investigation can be pointed out, such as the difficulty in locating the defects for laser irradiation. Besides, components of the P(VDF-TrFE)/BT membrane might have dispersed laser beam light, leading to insufficient deposition of total laser energy in bone defect site.

The initial hypothesis of our investigation was rejected due to the lack of significant improvements in bone repair after the association of photobiomodulation therapy with P(VDF-TrFE)/BT membrane evaluated by histological, morphometric, and molecular assays. Nevertheless, new studies should be performed with different photobiomodulation therapy protocols to evaluate a synergy between photobiomodulation and P(VDF-TrFE)/BT membrane. Results obtained in the present investigation suggest the protocol of photobiomodulation therapy utilized did not enhance bone repair when associated with P(VDF-TrFE)/BT. However, the utilization of texturized P (VDF-TrFE)/BT regardless of the association with photobiomodulation therapy enhanced bone repair in an experimental model of osteoporosis.

Acknowledgements We thank Adriana Luisa Gonçalves de Almeida and Sebastião Carlos Bianco for technical assistance during the experiments.

Author contribution Conceptualization: Fernanda Cristina Toloi Rufato, Marcio Mateus Beloti, Adalberto Luiz Rosa, Selma Siessere.

Methodology: Fernanda Crisitna Toloi Rufato, Priscilla Hakime Scalize, Luiz Gustavo de Sousa, Fabíola Singaretti de Oliveira, Rossano Gimenes, Isabela Hallak Regalo.

Formal analysis and investigation: Fernanda Crisitna Toloi Rufato, Luiz Gustavo de Sousa, Isabela Hallak Regalo, Simone Cecilio Hallak Regalo.

Writing—original draft preparation: Selma Siéssere, Rossano Gimenes, Karina Fittipaldi Bombonato-Prado.

Writing—review and editing: Karina Fittipaldi Bombonato-Prado, Rossano Gimenes, Simone Cecilio Hallak Regalo, Selma Siessere.

Funding acquisition: Selma Siéssere, Karina Fittipaldi Bombonato-Prado, Simone Cecilio Hallak Regalo.

Supervision: Selma Siessere.

Funding This study was supported by the São Paulo Research Foundation (FAPESP 2017/25683–4); Research and Support Foundation of Minas Gerais (FAPEMIG; Grant TEC-APQ-03013–15); and National Institute of Science and Technology, Translational Medicine, Brazil, and Coordination for the Improvement of Higher Education Personnel—Brazil (CAPES)—Finance Code 001.

Declarations

Ethics approval This investigation was approved by the Animal Research Committee (Protocol 2018.1.417.58.0.) of the School of Dentistry of Ribeirão Preto, University of São Paulo.

Informed consent For this type of study, formal consent is not required.

Conflict of interest The authors declare no competing interests.

References

1. Solomon CG, Black DM, Rosen CJ (2016) Postmenopausal osteoporosis. N Engl J Med 374:254–262. https://doi.org/10.1056/NEJMcp1513724
2. Kanis JA, McCloskey EV, Johansson H, Cooper C, Rizzoli R, Reginster JY (2013) European guidance for the diagnosis and management of osteoporosis in postmenopausal women. Osteoporos Int 24:23–57. https://doi.org/10.1007/s11657-013-0136-1
3. Straka M, Straka-Trapezanlidis M, Deglovic J, Varga I (2015) Periodontitis and osteoporosis. Neuro Endocrinol Lett 36:401–406
4. Otomo-Corgel J (2012) Osteoporosis and osteopenia: implications for periodontal and implant therapy. Periodontol 2000 59:111–139. https://doi.org/10.1111/j.1600-0757.2011.00435.x
5. Singh A, Sharma RK, Siwach RC, Tewari S, Narula SC (2014) Association of bone mineral density with periodontal status in postmenopausal women. J Investig Clin Dent 5:275–282. https://doi.org/10.1111/jicd.12047
6. Cybulska M, Głogowska-Szeląg J (2018) Periodontal diseases and risk of osteoporosis - case report. Wiad Lek 71:1841–1843
7. Daniell HW (1983) Postmenopausal tooth loss. Contributions to edentulism by osteoporosis and cigarette smoking. Arch Intern Med 143:1678–1682
8. Gur A, Nas K, Kayhan O, Atay MB, Akyuz G, Sindal D, Akşit R, Oncel S, Dilsen G, Cevik R, Gunduz OH, Ersoy Y, Altay Z, Ozturk C, Akkus S, Senocak O, Kavuncu V, Kirnap M, Tekeoglu I, Erdogan F, Sarac AJ, Demiralp L, Demirkesen A, Adam M (2003) The relation between tooth loss and bone mass in postmenopausal osteoporotic women in Turkey: a multicenter study. J Bone Miner Metab 21:43–47
9. Yoshihara A, Seida Y, Hanada N, Nakashima K, Miyazaki H (2005) The relationship between bone mineral density and the number of remaining teeth in community-dwelling older adults. J Oral Rehabil 32:735–740
10. Drozdzowska B, Pluskiewicz W, Michno M (2006) Tooth count in elderly women in relation to their skeletal status. Maturitas 55:126–131
11. Erdogan O, Incki KK, Benlidayi ME, Seydaoglu G, Kelekci S (2009) Dental and radiographic findings as predictors of osteoporosis in postmenopausal women. Geriatr Gerontol Int 9:155–164. https://doi.org/10.1111/j.1447-0594.2009.00518.x
12. Moedano DE, Irigoyen ME, Borges-Yáñez A, Flores-Sánchez I, Rotter RC (2011) Osteoporosis, the risk of vertebral fracture,

and periodontal disease in an elderly group in Mexico City. Gerodontology 28:19–27. https://doi.org/10.1111/j.1741-2358.2009.00342.x
13. Vargas-Sanchez PK, Pitol DL, de Sousa LG, Beloti MM, Rosa AL, Rossi AC, Siéssere S, Bombonato-Prado KF (2020) Green tea extract rich in epigallocatechin gallate impairs alveolar bone loss in ovariectomized rats with experimental periodontal disease. Int J Exp Pathol 101:277–288. https://doi.org/10.1111/iep.12379
14. Pinheiro ALB, Gerbi MEMM (2006) Photoengineering of bone process. Photomed Laser Surg 24:169–178. https://doi.org/10.1089/pho.2006.24.169
15. Dompe C, Moncrieff L, Matys J, Grzech-Leśniak K, Kocherova I, Bryja A, Bruska M, Dominiak M, Mozdziak P, Skiba THI, Shibli JA, Volponi AA, Kempisty B, Dyszkiewicz-Konwińska M (2020) Photobiomodulation-underlying mechanism and clinical applications. J Clin Med 9:1724. https://doi.org/10.3390/jcm9061724
16. Tim CR, Bossini PS, Kido HW, Malavazi I, von Zeska Kress MR, Carazzolle MF, Parizotto NA, Rennó AC (2015) Effects of low-level laser therapy on the expression of osteogenic genes during the initial stages of bone healing in rats: a microarray analysis. Lasers Med Sci 30:2325–2333. https://doi.org/10.1007/s10103-015-1807-5
17. Fallahnezhad S, Piryaei A, Darbandi H, Amini A, Ghoreishi SK, Jalalifirouzkouhi R, Bayat M (2018) Effect of low-level laser therapy and oxytocin on osteoporotic bone marrow-derived mesenchymal stem cells. J Cell Biochem 119:983–997. https://doi.org/10.1002/jcb.26265
18. Siessere S, de Sousa LG, Issa JP, Iyomasa MM, Pitol DL, Barbosa AP, Semprini M, Sebald W, Bentley MV, Regalo SC (2011) Application of low-level laser irradiation (LLLI) and rhBMP-2 in critical bone defect of ovariectomized rats: histomorphometric evaluation. Photomed Laser Surg 29:453–458. https://doi.org/10.1089/pho.2010.2917
19. Rosa AP, de Sousa LG, Regalo SC, Issa JP, Barbosa AP, Pitol DL, de Oliveira RH, de Vasconcelos PB, Dias FJ, Chimello DT, Siéssere S (2012) Effects of the combination of low-level laser irradiation and recombinant human bone morphogenetic protein-2 in bone repair. Lasers Med Sci 27:971–977. https://doi.org/10.1007/s10103-011-1022-y
20. Scalize PH, de Sousa LG, Regalo SC, Semprini M, Pitol DL, da Silva GA, de Almeida CJ, Coppi AA, Laad AA, Prado KF, Siessere S (2015) Low-level laser therapy improves bone formation: stereology findings for osteoporosis in rat model. Lasers Med Sci 30:1599–1607. https://doi.org/10.1007/s10103-015-1773-y
21. Retzepi M, Donos N (2010) Guided bone regeneration: biological principle and therapeutic applications. Clin Oral Implants Res 21:567–576. https://doi.org/10.1111/j.1600-0501.2010.01922.x
22. Dowell P, Moran J, Quteish D (1991) Guided tissue regeneration. Br Dent J 171:125–127
23. Gottlow J, Nyman S, Karring T (1992) Maintenance of new attachment gained through guided tissue regeneration. J Clin Periodontol 19:315–317
24. Laurell L, Gottlow J (1998) Guided tissue regeneration update. Int Dent J 48:386–398. https://doi.org/10.1111/j.1875-595x.1998.tb00701.x
25. Salata LA, Hatton PV, Devlin AJ, Brook IM, Craig G (2001) In vitro and in vivo evaluation of e-PTFE and alkali-cellulose membranes for guided bone regeneration. Clin Oral Implants Res 12:62–68
26. Walters SP, Greenwell H, Hill M, Drisko C, Pickman K, Scheetz JP (2003) Comparison of porous and non-porous teflon membranes plus a xenograft in the treatment of vertical osseous defects: a clinical reentry study. J Periodontol 74:1161–1168
27. Gimenes R, Zaghete MA, Bertolini M, Varela JA, Coelho LO, Silva NF Jr (2004) Composites PVDF-TrFE/BT used as bioactive membranes for enhancing bone regeneration. Proc SPIE Smart Struct Mater 5385:539–547
28. Lopes HB, Santos TS, de Oliveira FS, Freitas GP, de Almeida AL, Gimenes R, Rosa AL, Beloti MM (2014) Poly(vinylidene-trifluoroethylene)/barium titanate composite for in vivo support of bone formation. J Biomater Appl 29:104–112. https://doi.org/10.1177/0885328213515735
29. Scalize PH, Bombonato-Prado KF, de Sousa LG, Rosa AL, Beloti MM, Semprini M, Gimenes R, de Almeida AL, de Oliveira FS, Hallak Regalo SC, Siessere S (2016) Poly(vinylidene fluoride-trifluorethylene)/barium titanate membrane promotes de novo bone formation and may modulate gene expression in osteoporotic rat model. J Mater Sci Mater Med 27:180. https://doi.org/10.1007/s10856-016-5799-x
30. Gimenes R, Zaghete MA, Espanhol M, Sachs D, Silva MRA (2019) Promotion of bone repair of rabbit tibia defects induced by scaffolds of P(VDF-TrFE)/$BaTiO_3$ composites. Bull Mater Sci 42:235. https://doi.org/10.1007/s12034-019-1914-1
31. Kalu DN (1991) The ovariectomized rat model of postmenopausal bone loss. Bone Miner 15:175–191
32. Scalize PH, de Sousa LG, Gonçalves LMN, Pitol DL, Palinkas M, Coppi AA, Righeti MA, Ricardo V, Bombonato-Prado KF, Regalo SCH, Siessere S (2019) Low-level laser therapy enhances the number of osteocytes in calvaria bone defects of ovariectomized rats. Animal Model Exp Med 2:51–57. https://doi.org/10.1002/ame2.12056
33. Oliveira GR, Vargas-Sanchez PK, Fernandes RR, Ricoldi MST, Semeghini MS, Pitol DL, de Sousa LG, Siessere S, Bombonato-Prado KF (2019) Lycopene influences osteoblast functional activity and prevents femur bone loss in female rats submitted to an experimental model of osteoporosis. J Bone Miner Metab 37:658–667. https://doi.org/10.1007/s00774-018-0970-8
34. Johnston BD, Ward WE (2015) The ovariectomized rat as a model for studying alveolar bone loss in postmenopausal women. Biomed Res Int 2015:635023. https://doi.org/10.1155/2015/635023
35. Parfitt AM, Drezner MK, Glorieux FH, Kanis JA, Malluche H, Meunier PJ, Ott SM, Recker RR (1987) Bone histomorphometry: standardization of nomenclature, symbols, and units. Report of the ASBMR Histomorphometry Nomenclature Committee. J Bone Miner Res 2:595–610. https://doi.org/10.1002/jbmr.5650020617
36. Bouxsein ML, Boyd SK, Christiansen BA, Guldberg RE, Jepsen KJ, Müller R (2010) Guidelines for assessment of bone microstructure in rodents using micro-computed tomography. J Bone Miner Res 25:1468–1486. https://doi.org/10.1002/jbmr.141
37. Dempster DW, Compston JE, Drezner MK, Glorieux FH, Kanis JA, Malluche H, Meunier PJ, Ott SM, Recker RR, Parfitt AM (2013) Standardized nomenclature, symbols, and units for bone histomorphometry: a 2012 update of the report of the ASBMR Histomorphometry Nomenclature Committee. J Bone Miner Res 28:2–17. https://doi.org/10.1002/jbmr.1805
38. Maniatopoulos C, Rodriguez A, Deporter DA, Melcher AH (1986) An improved method for preparing histological sections of metallic implants. Int J Oral Maxillofac Implants 1:31–37
39. Sicchieri LG, Crippa GE, de Oliveira PT, Beloti MM, Rosa AL (2012) Pore size regulates cell and tissue interactions with PLGA-CaP scaffolds used for bone engineering. J Tissue Eng Regen Med 6:155–162. https://doi.org/10.1002/term.422
40. Livak KJ, Schmittgen TD (2001) Analysis of relative gene expression data using real-time quantitative PCR and the 2(-Delta Delta C(T)) method. Methods 25:402–408
41. Pinheiro AL, Aciole GT, Ramos TA, Gonzalez TA, da Silva LN, Soares LG, Aciole JM, dos Santos JN (2014) The efficacy of the use of IR laser phototherapy associated to biphasic ceramic graft and guided bone regeneration on surgical fractures treated with miniplates: a histological and histomorphometric study on

rabbits. Lasers Med Sci 29:279–288. https://doi.org/10.1007/s10103-013-1339-9
42. Linde A, Thoren C, Dahlin C, Sandberg E (1993) Creation of new bone by an osteopromotive membrane technique: an experimental study in rats. J Oral Maxillofac Surg 51:892–897. https://doi.org/10.1016/s0278-2391(10)80111-9
43. Karring T, Nyman S, Gottlow J, Laurell L (1993) Development of the biological concept of guided tissue regeneration-animal and human studies. Periodontol 2000 1:26–35
44. Mardas N, Busetti J, de Figueiredo JA, Mezzomo LA, Scarparo RK, Donos N (2017) Guided bone regeneration in osteoporotic conditions following treatment with zoledronic acid. Clin Oral Implants Res 28:362–371. https://doi.org/10.1111/clr.12810
45. Korzinskas T, Jung O, Smeets R, Stojanovic S, Najman S, Glenske K, Hahn M, Wenisch S, Schnettler R, Barbeck M (2018) In vivo analysis of the biocompatibility and macrophage response of a non-resorbable PTFE membrane for guided bone regeneration. Int J Mol Sci 19:2952. https://doi.org/10.3390/ijms19102952
46. Hamblin MR (2017) Mechanisms and applications of the anti-inflammatory effects of photobiomodulation. AIMS Biophys 4:337–361. https://doi.org/10.3934/biophy.2017.3.337
47. Freitas NR, Guerrini LB, Esper LA, Sbrana MC, Dalben GDS, Soares S, Almeida ALPF (2018) Evaluation of photobiomodulation therapy associated with guided bone regeneration in critical size defects. In vivo study. J Appl Oral Sci 26:e20170244. https://doi.org/10.1590/1678-7757-2017-0244
48. Rajabi AH, Jaffe M, Arinzeh TL (2015) Piezoelectric materials for tissue regeneration: a review. Acta Biomater 24:12–23. https://doi.org/10.1016/j.actbio.2015.07.010
49. Tandon B, Blaker JJ, Cartmell SH (2018) Piezoelectric materials as stimulatory biomedical materials and scaffolds for bone repair. Acta Biomater 73:1–20. https://doi.org/10.1016/j.actbio.2018.04.026
50. Teixeira LN, Crippa GE, Trabuco AC, Gimenes R, Zaghete MA, Palioto DB, de Oliveira PT, Rosa AL, Beloti MM (2010) In vitro biocompatibility of poly(vinylidene fluoride-trifluoroethylene)/barium titanate composite using cultures of human periodontal ligament fibroblasts and keratinocytes. Acta Biomater 6:979–989. https://doi.org/10.1016/j.actbio.2009.08.024
51. Fields AJ, Keaveny TM (2012) Trabecular architecture and vertebral fragility in osteoporosis. Curr Osteoporos Rep 10:132–140. https://doi.org/10.1007/s11914-012-0097-0
52. Karlamangla AS, Burnett-Bowie SM, Crandall CJ (2018) Bone health during the menopause transition and beyond. Obstet Gynecol Clin North Am 45:695–708. https://doi.org/10.1016/j.ogc.2018.07.012
53. de Jong TV, Moshkin YM, Guryev V (2019) Gene expression variability: the other dimension in transcriptome analysis. Physiol Genomics 51:145–158. https://doi.org/10.1152/physiolgenomics.00128.2018
54. Oliveira FA, Matos AA, Matsuda SS, Buzalaf MA, Bagnato VS, Machado MA, Damante CA, Oliveira RC, Peres-Buzalaf C (2017) Low level laser therapy modulates viability, alkaline phosphatase and matrix metalloproteinase-2 activities of osteoblasts. J Photochem Photobiol B 169:35–40. https://doi.org/10.1016/j.jphotobiol.2017.02.020
55. Golub EE, Boesze-Battaglia K (2007) The role of alkaline phosphatase in mineralization. Curr Opin Orthop 18:444–448. https://doi.org/10.1097/BCO.0b013e3282630851
56. Linder CH, Ek-Rylander B, Krumpel M, Norgård M, Narisawa S, Millán JL, Andersson G, Magnusson P (2017) Bone alkaline phosphatase and tartrate-resistant acid phosphatase: potential co-regulators of bone mineralization. Calcif Tissue Int 101:92–101. https://doi.org/10.1007/s00223-017-0259-2
57. Eghbali-Fatourechi G, Khosla S, Sanyal A, Boyle WJ, Lacey DL, Riggs BL (2003) Role of RANK ligand in mediating increased bone resorption in early postmenopausal women. J Clin Invest 111:1221–1230
58. Gordon JA, Tye CE, Sampaio AV, Underhill TM, Hunter GK, Goldberg HA (2007) Bone sialoprotein expression enhances osteoblast differentiation and matrix mineralization in vitro. Bone 41:462–473
59. Bailey S, Karsenty G, Gundberg C, Vashishth D (2017) Osteocalcin and osteopontin influence bone morphology and mechanical properties. Ann N Y Acad Sci 1409:79–84. https://doi.org/10.1111/nyas.13470
60. Walsh MC, Choi Y (2014) Biology of the RANKL-RANK-OPG system in immunity, bone, and beyond. Front Immunol 5:511. https://doi.org/10.3389/fimmu.2014.00511
61. Oliveira LSS, de Araújo AA, de Araújo Júnior RF, Barboza CAG, Borges BCD, da Silva JSP (2017) Low-level laser therapy (780 nm) combined with collagen sponge scaffold promotes repair of rat cranial critical-size defects and increases TGF-β, FGF-2, OPG/RANK and osteocalcin expression. Int J Exp Pathol 98:75–85. https://doi.org/10.1111/iep.12226
62. Mandelin J, Hukkanen M, Li TF, Korhonen M, Liljeström M, Sillat T, Hanemaaijer R, Salo J, Santavirta S, Konttinen YT (2006) Human osteoblasts produce cathepsin K. Bone 38:769–777. https://doi.org/10.1016/j.bone.2005.10.017
63. Debnath S, Yallowitz AR, McCormick J, Lalani S, Zhang T, Xu R, Li N, Liu Y, Yang YS, Eiseman M, Shim J, Hameed M, Healey JH, Bostrom MP, Landau DA, Greenblatt MB, MB, (2018) Discovery of a periosteal stem cell mediating intramembranous bone formation. Nature 562:133–139. https://doi.org/10.1038/s41586-018-0554-8
64. Dai R, Wu Z, Chu HY, Lu J, Lyu A, Liu J, Zhang G (2020) Cathepsin K: the action in and beyond bone. Front Cell Dev Biol 8:433. https://doi.org/10.3389/fcell.2020.00433
65. Zambuzzi WF, Yano CL, Cavagis AD, Peppelenbosch MP, Granjeiro JM, Ferreira CV (2009) Ascorbate-induced osteoblast differentiation recruits distinct MMP-inhibitors: RECK and TIMP-2. Mol Cell Biochem 322:143–150. https://doi.org/10.1007/s11010-008-9951-x
66. Tokuhara CK, Santesso MR, Oliveira GSN, Ventura TMDS, Doyama JT, Zambuzzi WF, Oliveira RC (2019) Updating the role of matrix metalloproteinases in mineralized tissue and related diseases. J Appl Oral Sci 27:e20180596. https://doi.org/10.1590/1678-7757-2018-0596
67. Lima LL, Gonçalves PF, Sallum EA, Casati MZ, Nociti FH Jr (2008) Guided tissue regeneration may modulate gene expression in periodontal intrabony defects: a human study. J Periodontal Res 43:459–464. https://doi.org/10.1111/j.1600-0765.2008.01094.x

Clinical relevance[A1][A1]note: article title

Authors and Affiliations

Fernanda Cristina Toloi Rufato[1] · Luiz Gustavo de Sousa[1] · Priscilla Hakime Scalize[1] · Rossano Gimenes[2] · Isabela Hallak Regalo[1] · Adalberto Luiz Rosa[3] · Marcio Mateus Beloti[1] · Fabíola Singaretti de Oliveira[3] · Karina Fittipaldi Bombonato-Prado[1] · Simone Cecilio Hallak Regalo[1] · Selma Siéssere[1]

Fernanda Cristina Toloi Rufato
fernandatoloifr@usp.br

Luiz Gustavo de Sousa
sousalg@forp.usp.br

Priscilla Hakime Scalize
priscillaid@hotmail.com

Rossano Gimenes
rossano@unifei.edu.br

Isabela Hallak Regalo
isabelahregalo@usp.br

Adalberto Luiz Rosa
adalrosa@forp.usp.br

Marcio Mateus Beloti
mmbeloti@usp.br

Fabíola Singaretti de Oliveira
oliveira@forp.usp.br

Karina Fittipaldi Bombonato-Prado
karina@forp.usp.br

Simone Cecilio Hallak Regalo
simone@forp.usp.br

[1] Department of Basic and Oral Biology, School of Dentistry of Ribeirão Preto, University of São Paulo, Avenida Do Café S/N, Ribeirão Preto, SP 14040-904, Brazil

[2] Institute of Physics and Chemistry, Federal University of Itajubá, Itajubá, MG, Brazil

[3] Department of Oral and Maxillofacial Surgery and Periodontology, School of Dentistry of Ribeirão Preto, University of São Paulo, Ribeirão Preto, SP, Brazil